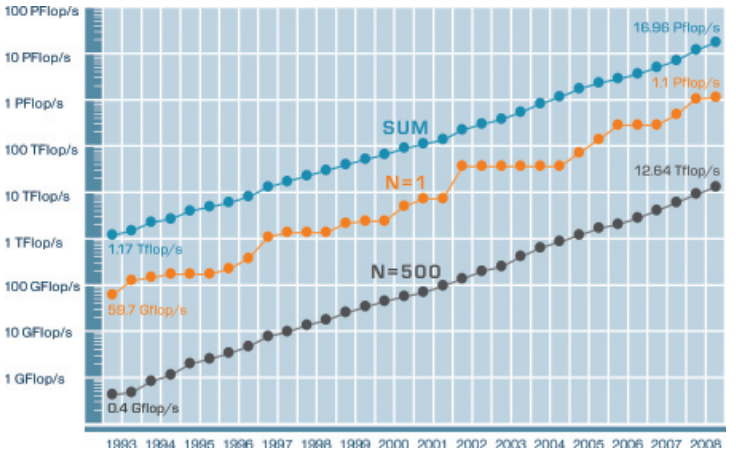

Figure 1.1 Computing speed of the 500 fastest computers in the world (Top500, 2008).

(a)

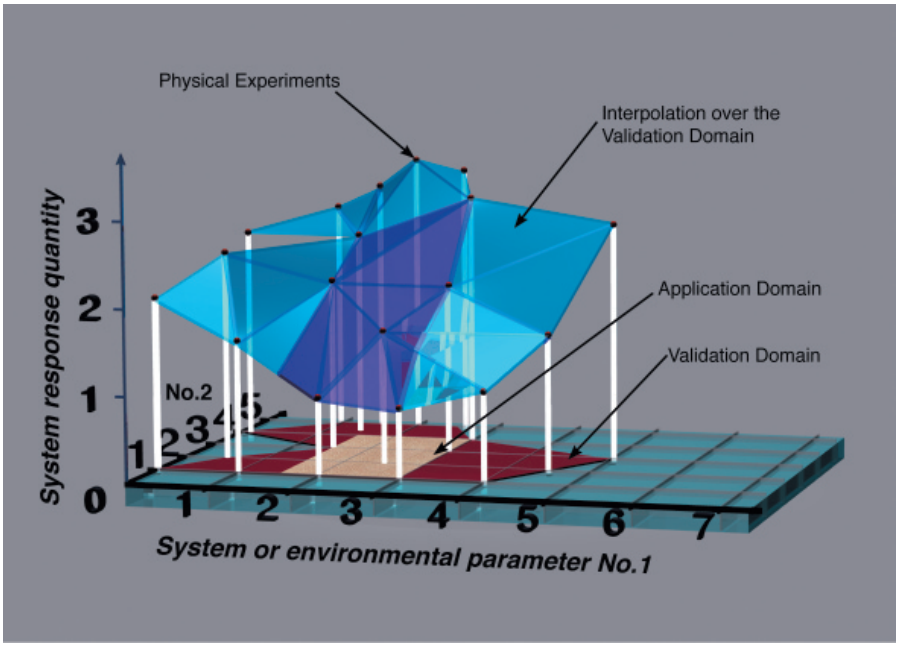

(b)

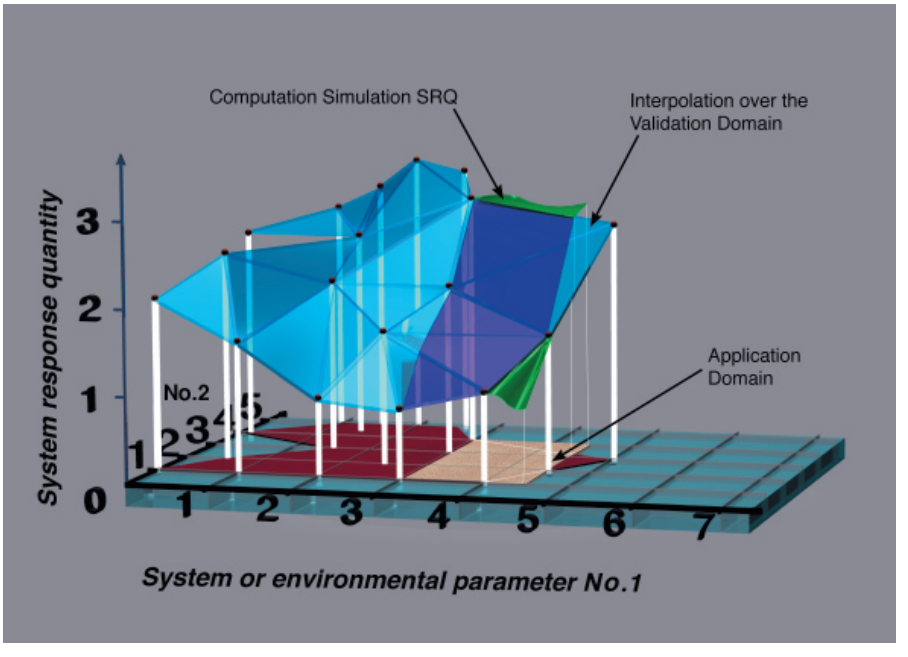

Figure 2.10 Possible relationships of the validation domain to the application domain.

(c)

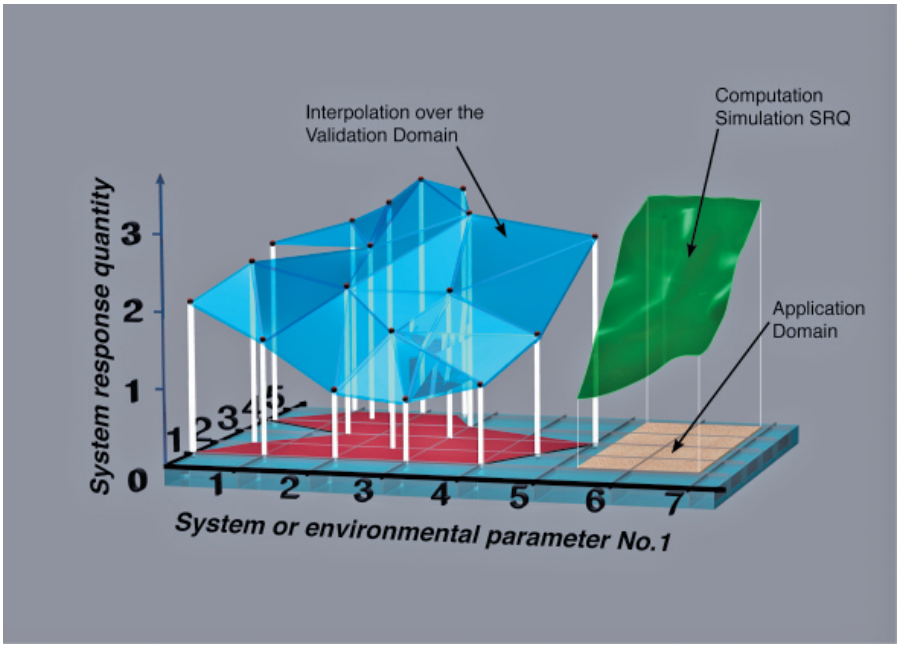

Figure 2.10 (*cont.*)

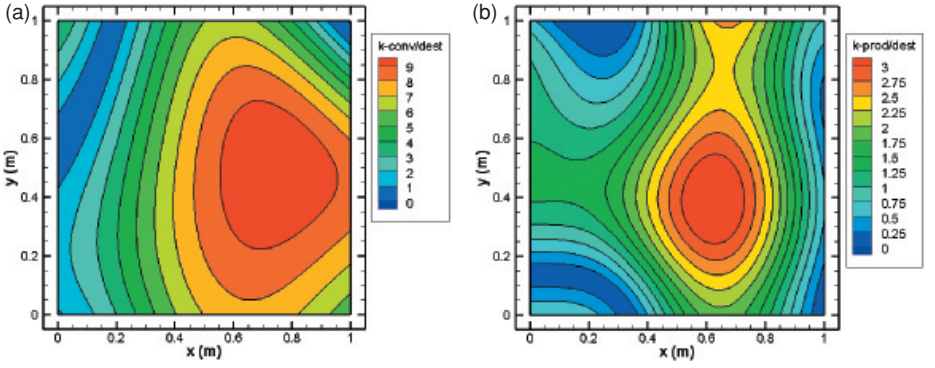

Figure 6.5 Ratios of (a) the convection terms and (b) the production terms to the destruction terms for a turbulent kinetic energy transport equation (from Roy *et al*., 2007b).

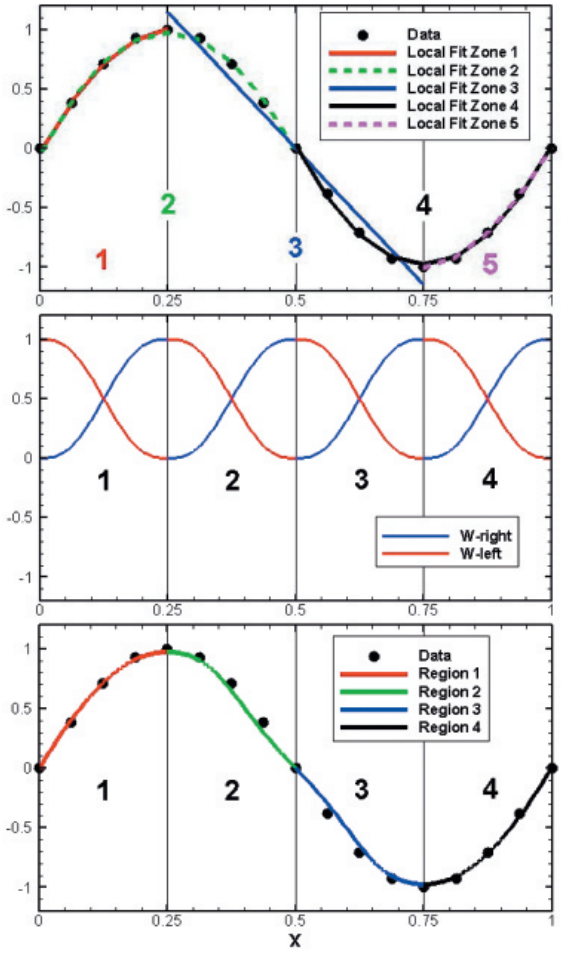

Figure 6.16 Simple one-dimensional example of the weighting function approach for combining local quadratic least squares fits to generate a C^2 continuous spline fit: local fits (top), weighting functions (middle), and resulting C^2 continuous spline fit (bottom) (from Roy and Sinclair, 2009).

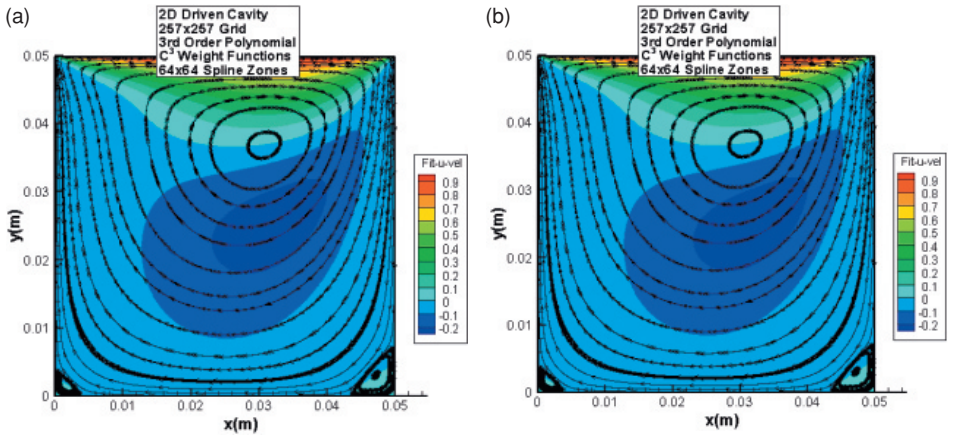

Figure 6.17 Contours of u-velocity and streamlines for a lid-driven cavity at Reynolds number 100: (a) 257×257 node numerical solution and (b) C^3 continuous spline fit using 64×64 spline zones (from Roy and Sinclair, 2009).

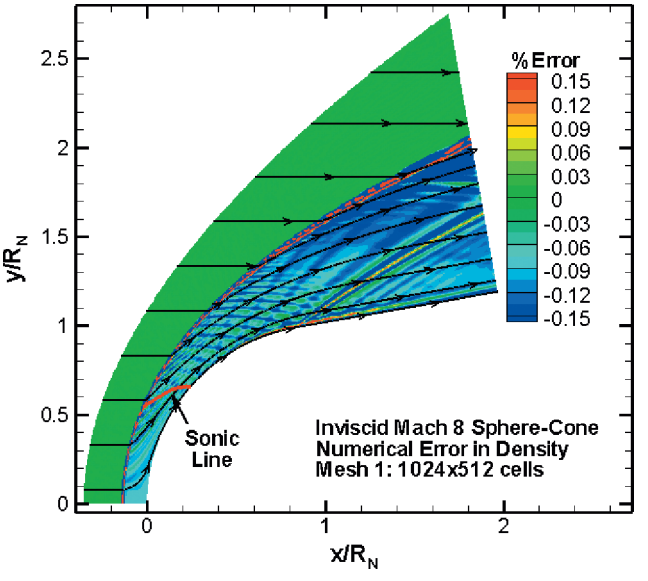

Figure 8.1 Contours of total estimated discretization error in density for the flow over an inviscid hypersonic sphere cone (from Roy, 2003).

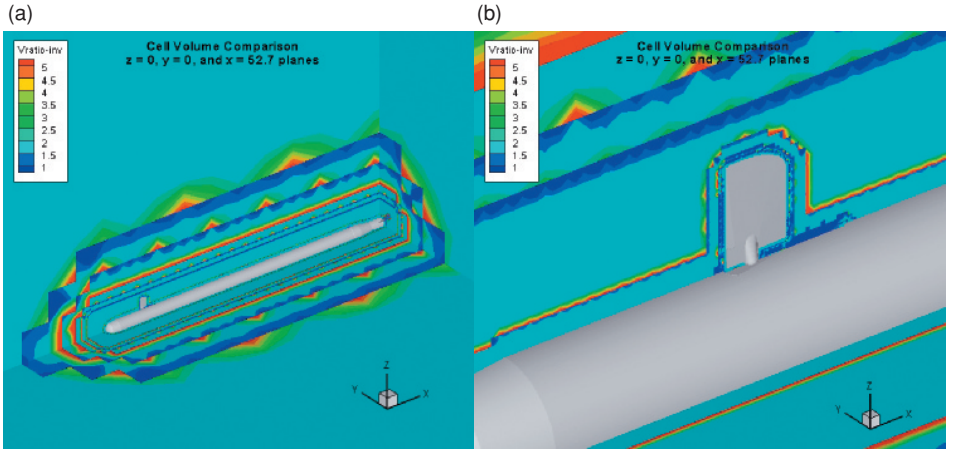

Figure 8.12 Contour plots of the cell volume ratio between the two unstructured Cartesian mesh levels for (a) the entire missile geometry and (b) a close-up of the canard (from Roy *et al.*, 2007).

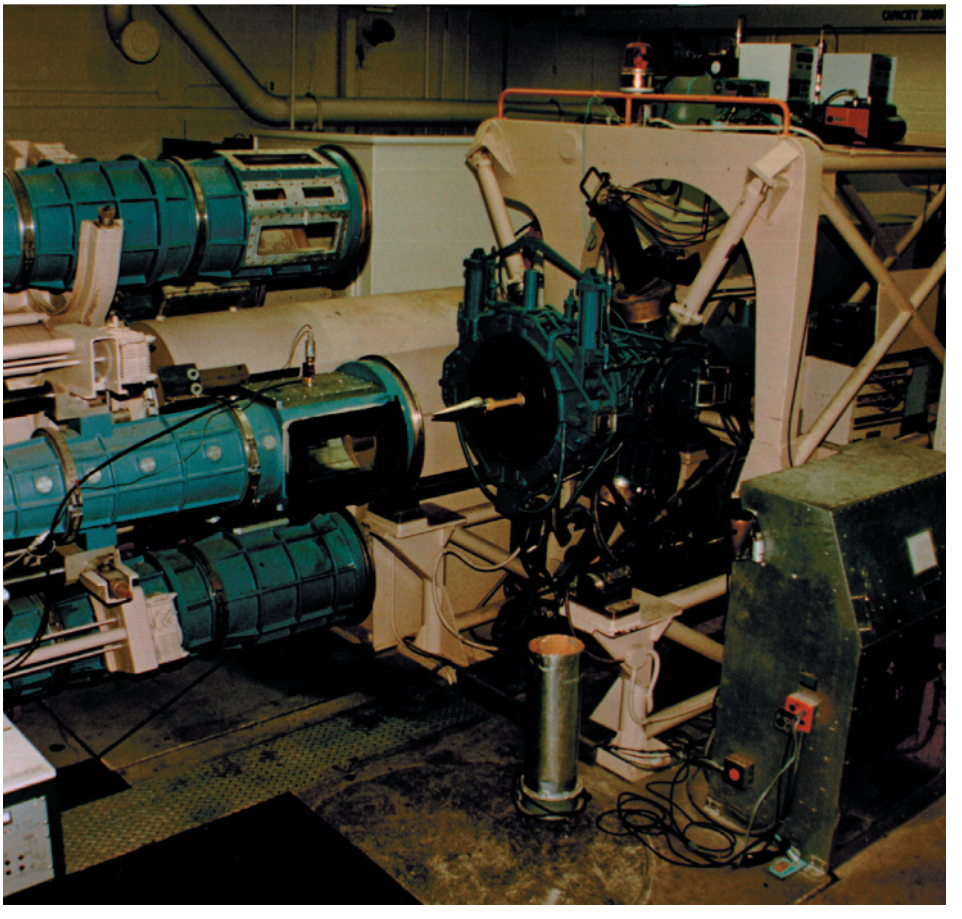

Figure 11.2 Sandia hypersonic wind tunnel with the aft section retracted from the test section (flow is from left to right). The model is visible in the open section and the yellow support is part of the rear-mounting fixture to hold the model (Oberkampf *et al.*, 1993).

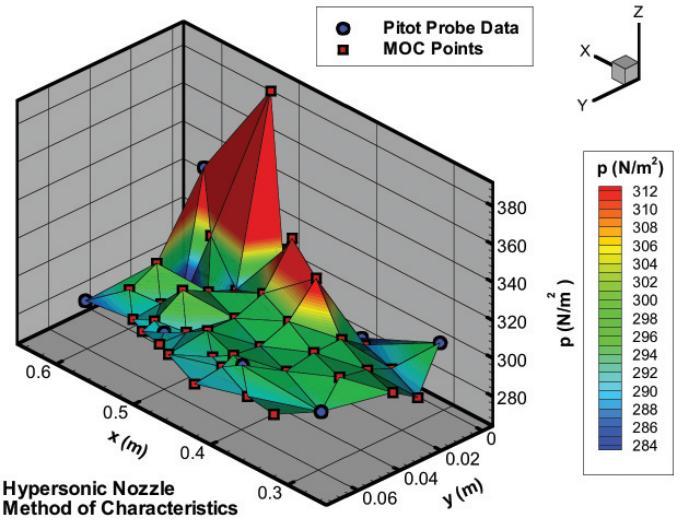

Figure 11.14 Free-stream static pressures from a combination of flowfield calibration data and MOC generated data (Roy *et al.*, 2003).

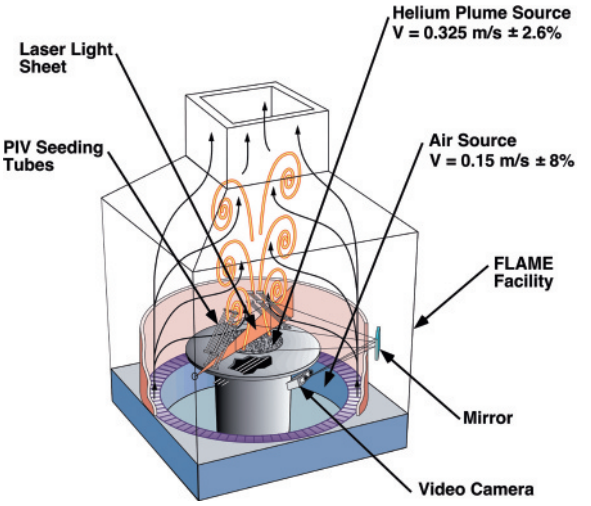

Figure 12.7 Experimental setup for measurements of the helium plume (O'Hern *et al.*, 2005).